Contrib Mineral Petrol (2001) 141: 546–559
DOI 10.1007/s004100100258

Monika Koch-Müller · Richard Wirth

An experimental study of the effect of iron on magnesiochloritoid-talc-clinochlore-kyanite stability

Received: 7 March 2000 / Accepted: 13 February 2001 / Published online: 12 May 2001

Abstract The influence of Fe on the reaction clinochlore + kyanite + magnesiochloritoid + talc (1) was determined experimentally as a function of pressure (1.6–2.6 GPa) and composition at 600 and 540 °C. Analytical electron microscopy (AEM) was used to determine the compositions of the coexisting phases in these complex multiphase run products. Within the compositional range studied ($x_{Fe}^{bulk} = 0.12$–0.34), chlorite solid solutions were always richer in magnesium than the coexisting chloritoid solid solutions. Fractionation of Fe into the chloritoid extends the stability field of the assemblage chloritoid plus talc towards lower pressures. However, the extent of the stability field for increasing x_{Fe} is less than one would expect for ideal mixing behaviour in chloritoid and chlorite, and indicates a moderate positive deviation from ideality for chloritoid solid solutions. The thermodynamic data for magnesiochloritoid given in two earlier studies are in good agreement with the present experiments, those of a third study yield pressures which are much too high, at least compared with the experiments at 600 °C.

M. Koch-Müller (✉)
Technische Universität Berlin,
Institut für Angewandte Geowissenschaften I,
BH1, Ernst-Reuter-Platz 1, 10587 Berlin, Germany
E-mail: monika.koch-muller@gl.ciw.edu
Tel.: +202-4788931
Fax: +202-4788901

R. Wirth
GeoForschungsZentrum Potsdam,
Telegrafenberg, Projektbereich 4.1,
14473 Potsdam, Germany

Present address: M. Koch-Müller
Geophysical Laboratory CHiPR,
Carnegie Institution of Washington,
5251 Broad Branch Road, N.W.,
Washington, DC 20015-1305, USA

Editorial responsibility: W. Schreyer

Introduction

A remarkable feature in high-pressure metapelitic and metagabbroic rocks is the relative abundance of Mg-rich chloritoid which may coexist with talc, kyanite, chlorite and garnet. Mg-rich chloritoid is known as a key mineral for blueschist-facies rocks, i.e. rocks which were subducted to depths greater than 35 km (1 GPa) at low geothermal gradients of 5–9 °C km^{-1} (Chopin 1983; Schreyer 1988; Chopin 1990). Terrains which represent such thermal regimes are widespread in the Alps and the Mediterranean region. Magnesiochloritoid occurs, for example, in eclogitic metapelite of the high-pressure metamorphic terrains of the Western Alps such as the Monte Rosa, Gran Paradiso and Dora-Maira Massifs, Italy (Chopin 1983; Chopin and Monié 1984; Simon et al. 1997), and the eclogitic zone of the Tauern Window, Austria (Miller 1977). Another type of occurrence is found in high-pressure veins in metabasites and ultramafic rocks, e.g. the ophiolite zone of Zermatt-Saas Fee (Bearth 1963), the Allalin Gabbro (Chinner and Dixon 1973; Meyer 1983), the Lanzo peridotite body (Kiénast and Pognante 1988), and the Ligurian Western Alps (Messiga et al. 1995). The Mg content of chloritoids in high-P metagabbro usually does not exceed 70 mol% of the Mg-end member; in metapelite, chloritoids with higher Mg contents ranging from 65 to 90 mol% are observed. The most magnesian-rich chloritoid reported so far contains 97 mol% of the Mg-end member (Simon et al. 1997). Chopin (1983, 1990), Chopin and Schreyer (1983), and Simon et al. (1997) have demonstrated that the Mg content of chloritoid coexisting with, for example, clinochlore-kyanite-talc or clinochlore-quartz-talc is essentially pressure dependent. Thus, the Mg content of chloritoid may be used to estimate the pressure of formation (e.g. Meyer 1983; Simon et al. 1997; Messiga et al. 1999).

Phase relations found in magnesiochloritoid-bearing rocks are shown in Fig. 1. Reactions (4) to (7) are metastable in the pure magnesian system, since Mg

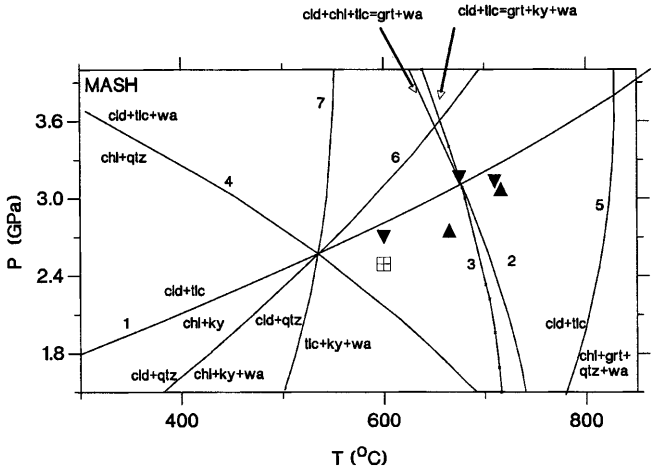

Fig. 1 Calculated P-T diagram in the MASH system, showing some phase relations found in magnesiochloritoid-bearing rocks. Calculations were performed using the package GE0-Calc (Brown et al. 1988), the thermodynamic data set of Berman (1988, updated), and data for magnesiochloritoid given in Simon et al. (1997). Both stable and metastable curves are presented. In addition, half brackets and brackets for reaction (1) as determined by Chopin (1985) are shown: *closed triangles* (*inverted closed triangles*) growth of chl and ky (growth of cld and tlc); *crossed square* no reaction. The following mineral formula were used: cld $MgAl_2SiO_5(OH)_2$; chl $Mg_5Al_2Si_3O_{10}(OH)_8$; tlc $Mg_3Si_4O_{10}(OH)_2$; grt $Mg_3Al_2Si_3O_{12}$; ky Al_2SiO_5; qtz SiO_2

chloritoid is not compatible with a SiO_2 phase (Chopin and Schreyer 1983; Schreyer 1988). Among reactions (1) to (7), reaction (1) (Abbreviations after Kretz 1983)

$$2\text{chl} + 5\text{ky} = 7\text{cld} + 1\text{tlc}$$

is of greatest geobarometric interest due to its relatively flat P–T slope (Chopin 1985; Chopin and Schreyer 1983) and its independence on f_{H2O}. The Mg end-member reaction (1) has been experimentally determined by Chopin (1985; Fig. 1). However, no data exist in the FMASH system. Assuming ideal mixing for chlorite and chloritoid, Simon et al. (1997) showed that Mg end-member reaction (1) is shifted dramatically towards lower pressure with increasing Fe incorporation into chlorite and chloritoid, so that reaction (1) would have a great potential as a geobarometer. For clinochlore-chamosite solid solutions it has been shown that deviation from ideality is – if at all – negligible (Bryndzia and Scott 1987; McPhail et al. 1990; Saccocia and Seyfried 1994; Holland et al. 1998). However, spectroscopic investigation of synthetic Fe-Mg chloritoid (Koch-Müller et al. 2000) indicated that chloritoid solid solutions may not behave ideally. Thus, experiments investigating the mixing behaviour of chloritoid are needed to fully develop the geobarometric potential of reaction (1) in natural rocks.

The aim of this study was to experimentally determine the position of reaction (1) in the FMASH system as a function of P, T and x, and to estimate the Fe-Mg mixing behaviour of cld solid solutions. Attempts to measure the compositions of the run products by means of an electron microprobe failed due to insufficient sample polish. We experienced that it is nearly impossible to polish a mixture of the phases of reaction (1), consisting of chlorite, chloritoid, talc and kyanite, sufficiently well for electron microprobe analyses. Therefore, we used transmission electron microscopy (TEM) in combination with X-ray analysis (AEM) to determine the chemical composition of the run products. Although AEM has been known for many years (e.g. Lorimer and Champness 1973), up to now only a few experimentalists have used it to characterise their run products (Dupas et al. 1994; Martinez et al. 1997; Meissner et al. 1998). The present study demonstrates that AEM is a suitable technique to determine quantitatively the phase compositions in a multiphase run product whose mineral composition can otherwise only be determined by indirect methods. However, even the use of an electron microscope with its high magnification does not necessarily prevent mixed analyses, and a careful examination of the measurements is required. Unfortunately, the studied system is very complex and the data obtained allow only an estimate of the thermodynamic behaviour of chloritoid.

Experimental methods

Experimental strategy

The aim of this study was to experimentally determine the effect of Fe on the magnesiochloritoid–talc–clinochlore–kyanite stability. According to the experiments of Chopin (1985), the Mg end-member reaction 2 clinochlore + 5 kyanite = 7 magnesiochloritoid+ 1 talc occurs between 2.5 and 2.7 GPa at a temperature of 600 °C. In the FMASH system the reaction becomes divariant and iron incorporates preferably into the coexisting chloritoid and chlorite, with chlorite solid solutions always richer in magnesium than the coexisting chloritoid solid solutions (Thompson 1976). The Fe-Mg exchange between chlorite and chloritoid can be described by reaction (EX)

$$\frac{1}{5}\text{Fe}_5\text{Al}[(\text{AlSi}_3\text{O}_{10})/(\text{OH})_8] + \text{MgAl}_2[\text{O}/(\text{SiO}_4)/(\text{OH})_2] = \frac{1}{5}\text{Mg}_5\text{Al}[(\text{AlSi}_3\text{O}_{10})/(\text{OH})_8] + \text{FeAl}_2[\text{O}/(\text{SiO}_4)/(\text{OH})_2] \quad \text{(EX)}$$

However, incorporation of Fe into the chloritoid and chlorite phases does not only cause a fractionation of Fe into chloritoid but it also extends the stability field of chloritoid plus talc to lower pressures. In addition to reaction (EX), reaction (1), the breakdown of chloritoid plus talc to chlorite plus kyanite, for example, is valid:

The experiments were performed with stoichiometric mixtures according to reaction (1) of natural kyanite and talc plus synthetic chloritoid and chlorite of different composition held for a certain

$$\underset{\text{talc(tlc)}}{\text{Mg}_3[\text{Si}_4\text{O}_{10}/(\text{OH})_2]} + \underset{\text{chlorotoid(cld)}}{7\,(\text{Mg},\text{Fe})\text{Al}_2[\text{O}/(\text{SiO}_4)/(\text{OH})_2]} = \underset{\text{chlorite(chl)}}{2\,(\text{Mg},\text{Fe})_5\text{Al}[(\text{AlSi}_3\text{O}_{10})/(\text{OH})_8]} + \underset{\text{kyanite(ky)}}{5\,\text{Al}_2[\text{O}/\text{SiO}_4]} \quad (1)$$

time at a constant pressure and temperature. Depending on the bulk composition of the starting material, the amount of chloritoid plus talc (or chlorite plus kyanite) changes during the runs, and Fe and Mg may exchange between chlorite and chloritoid. The bulk compositions of the starting material were chosen in order to reverse the runs and to ensure the presence of all four phases after the runs. Unfortunately, the system is very complex since chlorite may deviate from the clinochlore–chamosite solid solution, and talc may incorporate Fe and/or Al as a function of P and T. For example, natural talc found in HP assemblages may contain up to 1.5 wt% Al_2O_3 and 2 wt% FeO (e.g. Chinner and Dixon 1973 ; Simon et al. 1995; Messiga et al. 1999). Thus, after the run the presence and compositions of all four phases in the run products have to be checked carefully.

Preparation of starting materials

Fe-Mg-chloritoid and Fe-Mg-chlorite solid solutions of different compositions were synthesised at the Technische Universität Berlin in a piston-cylinder apparatus using rock-salt cells at 2.0–2.5 GPa and about 600 °C for chloritoid, and 1.0–2.0 GPa and 600–700 °C for chlorite. The solid solutions were synthesised with water in excess from stoichiometric mixtures of synthetic FeO (reacted from a stoichiometric mixture of Fe and Fe_2O_3 in evacuated quartz-glass ampoules), MgO p.a. (Merck), noncrystalline SiO_2 (aerosil 200, Degussa, heated at 1,000 °C for 48 h), and γ-Al_2O_3 (reacted from 99.95% Al foil from Merck). Run duration was 48 h in each case. The runs were buffered at the oxygen fugacity defined by the wüstite/iron buffer (WI). For a detailed description of the experimental setup see Koch-Müller (1997).

Fe-Mg exchange runs

The exchange runs were performed at the Technische Universität Berlin in a piston-cylinder apparatus. Synthetic chloritoid and chlorite solid solutions were mixed with natural end-member talc and kyanite proportional to the stoichiometry of reaction (1).

Ten to 20 mg of a mixture according to reaction (1) was sealed with 1–2 µl H_2O in $Ag_{70}Pd_{30}$ capsules, 4 mm long and 3 mm in diameter. Two of these inner capsules were placed on top of each other in the centre of an iron capsule which was 5.5 mm in diameter and 10 mm long. A detailed description of the experimental setup is given in Koch-Müller (1997). Table 1 summarises the conditions of the experiments. Experiments were performed at 540 and 600 °C in the pressure range of 1.6 to 2.6 GPa. The run duration was limited to a maximum of 116 h due to the consumption of the buffer material during the run.

Analytical methods

The run products were analysed by optical microscopy, electron microprobe (starting material), X-ray powder diffractometry (starting material and exchange products), infrared spectroscopy (starting material and some exchange runs), analytical transmission electron microscopy (some starting materials, exchange products), and Mössbauer spectroscopy (some of the starting materials).

For electron microprobe (EMP) analyses the starting materials chloritoid, chlorite, kyanite and talc were embedded separately in epoxy and polished. The measurements were performed with a Cameca Camebax at the ZELMI laboratory of the Technische Universität Berlin, and with Cameca SX50 and SX100 microprobes at the GeoForschungsZentrum Potsdam, using the wavelength dispersive mode. Operating conditions were 15 kV and 15 nA. Counting time was set at 20 s on peak and 10 s on background. Well-characterised natural minerals were used as standards: andalusite, wollastonite (Si), andalusite, K-feldspar (Al), olivine (Mg), hematite, metallic iron (Fe), spessartine (Mn), willemite (Zn), rutile (Ti) and chromite (Cr). Raw spectrometer data were corrected with the PAP program (Pouchou and Pichoir 1985).

The powder X-ray diffraction (XRD) patterns of the starting materials and the products were recorded in transmission mode, using a fully automated STOE STADI P diffractometer ($CuK\alpha_1$ radiation, 40 kV and 40 mA) equipped with a primary Ge monochromator and a 7°-wide position sensitive detector (PSD). The samples were fixed between Mylar foils. The X-ray powder patterns were recorded from 5–125° 2 θ in steps of 0.02°. Counting times were selected to yield a maximum intensity of 2,000–3,000 counts. Unit cell parameters of the starting materials were refined using the GSAS software package for Rietveld refinements (Larson and Von Dreele 1998). The reaction progress of the runs was estimated using a semiquantitative method based on changes in the following intensity ratios of X-ray reflections: $\frac{I^{cld}_{d(\bar{1}\bar{1}1),(\bar{2}01)}}{I^{chl}_{d(002)}}$, $\frac{I^{cld}_{d(\bar{1}\bar{1}1),(\bar{2}01)}}{I^{chl}_{d(004)}}$ and $\frac{I^{cld}_{d(\bar{1}\bar{1}1),(\bar{2}01)}}{I^{chl}_{d(201)}}$. The intensity ratios of these peaks, for a starting mixture with 40.4 wt% chloritoid ($x_{Fe}=0.30$), 29.7 wt% chlorite ($x_{Fe}=0.10$), 20.2 wt% kyanite and 9.6 wt% talc corresponding to reaction (1), were determined experimentally as 3.2, 2.7 and 2.9. The intensity ratios of these peaks were determined for each run product. An increase of these values by 10% was taken as chloritoid plus talc growth, and a decrease of the values by 10% as chlorite plus kyanite growth. Calculated powder pattern (PowderCell, Kraus and Nolze 1999), using different compositions for chloritoid and chlorite, showed that changes in the composition of the phases has only little effect on the calculated intensity ratios – at least for the composition range observed in this study.

To prove the presence of talc in some run products, powder IR spectra were performed. For this purpose, 2 mg of an initial four-phase mixture and 1–1.5 mg of the exchange run products 98-25 and 98-42 was mixed with about 100 mg KBr. The spectra were recorded on a Bruker IFS 66 FTIR spectrometer equipped with a Globar light source, a KBr beamsplitter, and a DTGS detector. The operating conditions for the spectrometer were 2 cm^{-1} resolution and 128 averaged scans.

Table 1 Listing of experimental conditions of the exchange runs

Run no.	P (GPa)	T (°C)	D (h)	Reactants			
				Run no.	x^{cld}_{Mg}	x^{chl}_{Mg}	Bulk x^{a}_{Mg}
97-11[b]	2.5	600	72	97-1		1.00	0.88
				97-6	0.65		
97-13[b]	2.6	600	72	97-9		0.90	0.83
				97-6	0.65		
98-12	2.3	600	72	98-10		0.78	0.75
				97-17	0.61		
98-13	2.3	600	72	98-10		0.78	0.71
				97-4	0.49		
98-25[b]	2.1	600	96	97-9		0.90	0.82
				98-23	0.64		
98-26[b]	2.1	600	96	98-10		0.78	0.72
				98-4	0.56		
99-7	1.9	600	116	99-1		0.74	0.66
				99-2	0.40		
98-41[b]	2.0	540	96	98-10		0.78	0.78
				98-23	0.64		
98-42	2.0	540	96	97-1		1.00	0.80
				98-32	0.43		
98-27[b]	1.8	540	96	97-9		0.90	0.82
				98-23	0.64		
98-29[b]	1.8	540	96	98-10		0.78	0.74
				98-4	0.56		
99-5	1.6	540	116	99-1		0.74	0.66
				99-2	0.40		

[a] $x_{Mg} = (7 * x^{cld}_{Mg} + 3 * x^{tlc}_{Mg} + 2 * 5 * x^{chl}_{Mg})/20$ according to the reaction $7(Mg,Fe)Al_2[O/(SiO_4)/(OH)_2] + Mg_3[Si_4O_{10}/(OH)_2] = 2(MgFe)_5Al[(AlSi_3O_{10})/(OH)_8] + 5Al_2[O/SiO_4]$

[b] Mixture contains 1–2 mol% staurolite as additional phase

Mössbauer spectra of some chloritoid starting materials and one Fe-rich chlorite sample were obtained at the Technische Universität Berlin, using a Mössbauer spectrometer (driving unit and MCA from Haleder Electronic, FRG) equipped with a source of ^{57}Co in Pd. Experimental details are given in Koch-Müller et al. (2000). The program package Recoil (Lagarec and Rancourt 1998) was used to perform a Voigt-based fitting analysis.

The run products for the analytical transmission electron microscopy (AEM) measurements were ground and suspended in ethanol by ultrasonic treatment and then transferred from the suspension onto a carbon 100-mesh grid. They were slightly coated with carbon to prevent charging in the TEM. Heating of the grid by using a 100-W electric bulb reduced contamination in the TEM significantly. AEM analyses were carried out on the run products, including chloritoid, chlorite and some talc and kyanite. The measurements were done at the GeoForschungsZentrum Potsdam, using a Philips CM200 TEM in twin-objective lens configuration. The TEM was operated at 200 kV with a LaB_6 filament as electron source. An energy dispersive EDAX X-ray analyser with an ultrathin window and an energy resolution of 143 eV was used for AEM. Chemical analyses were carried out in transmission mode with a nominal spot size of 55 nm. Defocusing the beam prevents the sample from loosing volatile elements such as Mg during the analyses (Peacor 1993). Specimen tilt towards the detector was 20°, measuring time 120 s.

All spectra were corrected for absorption and fluorescence, applying the EDAX software package. The specimen thickness necessary for absorption correction was determined by electron energy-loss spectroscopy (EELS), using the total intensity of the electrons reaching the EEL spectrometer and the intensity of the zero-loss peak (Egerton 1996). The specimen thickness (t) is given by the expression $t = \lambda * \ln(I_t/I_O)$, with I_t being the total intensity, I_o the intensity of the zero-loss peak, and λ the mean free path of the electrons in the specimen. The mean free path for 200-keV electrons in chloritoid was estimated to be 117 nm (e.g. Malis et al. 1988; Egerton 1996). The EELS spectra were acquired with a Gatan imaging filter GIF.

EDX analyses were quantified using the ratio technique of Cliff and Lorimer (1975) where $c_a/c_{Si} = k_{a,Si} * (I_a/I_{Si})$. For chloritoid, chlorite and talc the $k_{a,Si}$ factors k_{FeSi}, k_{AlSi}, k_{MnSi} and k_{MgSi} were determined from synthetic and natural chloritoid and chlorite standard materials which have been measured by electron microprobe. For kyanite the k_{AlSi} and k_{FeSi} factors were determined using a natural well-characterised kyanite (sample U-158; Platonov et al. 1998). At least 50 different measurements were carried out at different locations in the same standard foil. The standards were measured using the same microscope parameters as those used for the samples. The precision of the analyses depends on counting statistics ($\sigma=\sqrt{N}$, N = number of counts), the number of measurements, and the errors in k_{ab} values. The relative error for $k_{a,Si}$ is $k_{Mg/Si} = 2.4\%$ rel., $k_{Al/Si} = 1.3\%$ rel., $k_{Fe/Si} = 2.3\%$ rel. and $k_{Mn/Si} = 4.9\%$ rel. The relative error in the analysis is the sum of relative error in k_{AB} and the relative error of the determination of the composition. The relative errors for SiO_2, Al_2O_3, FeO and MgO are 3.9, 1.8, 2.8 and 8.2% respectively.

The accuracy of the measurements was checked by measuring the standards and comparing the results with the EMP analyses. Table 2 compares the electron microprobe analyses of the standard material with the AEM analyses, using the experimentally determined k factors. There is a good agreement between both sets of analyses. At least 30 measurements per sample were done on coexisting chloritoid and chlorite phases of the exchange runs. Figure 2 shows the products of run 98-41 with typical hexagonal crystal shapes for both minerals, chlorite and chloritoid. They can be distinguished only by chemical analysis. Mixed analyses due to phase overlap could be detected by plotting the analytical data in a SiO_2-Al_2O_3-(FeO,MgO) triangle. Figure 3 shows the analyses of run product 97-11. This presentation shows that chloritoid compositions tend towards talc, indicating analyses of talc and chloritoid mixtures. Only analyses close to the ideal chloritoid composition were accepted. Such triangles as well as Al_2O_3-FeO-MgO triangles were plotted for all run products, and the data were carefully analysed. The amount of talc in the run product is very low (up to 2 wt% only), and it was nearly impossible to get a reasonable analyses of this phase. Occasionally (97-13, 98-41, 98-42), very thin (< 10Å) sheets of a Mg- and Si-rich phase could be found whose compositions plot close to the ideal talc composition.

Results and discussion

Starting material

Table 3 lists the electron microprobe analyses of the kyanite, talc, chlorite and some chloritoid starting ma-

Table 2 Comparison of EMP and AEM analyses of selected standard materials. The formulae were calculated on the basis of 12 oxygens (cld) and 14 oxygen (chl). EMP analyses were calculated to 100% for comparison. *Values in parentheses* 1 σ standard deviation. *Ns* Number of analyses

Run no.	97-10		97-6		Nat cld		99-1	
	Chloritoid		Chloritoid		Chloritoid		Chlorite	
	EMP	AEM	EMP	AEM	EMP	AEM	EMP	AEM
Ns	15	10	15	10	15	10	15	10
Wt%								
SiO_2	27.79 (35)	27.60 (89)	29.13 (35)	29.40 (78)	26.57 (29)	27.20 (85)	36.70 (79)	36.30 (98)
Al_2O_3	45.12 (53)	45.10 (70)	47.07 (33)	47.20 (70)	43.70 (20)	44.00 (48)	23.35 (40)	23.10 (71)
FeO	20.42 (38)	20.80 (56)	11.66 (36)	11.60 (40)	27.06 (25)	26.30 (30)	14.82 (71)	15.70 (30)
MgO	6.65 (18)	6.50 (41)	12.11 (29)	11.90 (22)	2.25 (25)	2.30 (30)	25.14 (65)	24.90 (43)
MnO	0.00	0.00	0.00	0.00	0.42 (5)	0.20 (8)	0.00	0.00
Σ	100.00	100.00	100.00	100.00	100.00	100.00	100.00	100.00
Apfu								
Si	2.05 (2)	2.05 (4)	2.07 (3)	2.08 (5)	2.04 (2)	2.07 (4)	3.10 (2)	3.15 (8)
$Al^{(4)}$	0.00	0.00	0.00	0.00	0.00	0.00	0.90 (4)	0.85 (4)
$Al^{(6)}$	3.93 (2)	3.94 (3)	3.93 (4)	3.93 (4)	3.96 (2)	3.95 (4)	1.43 (4)	1.48 (4)
Fe^{2+}	1.26 (4)	1.29 (4)	0.69 (2)	0.69 (3)	1.71 (2)	1.67 (5)	1.13 (6)	1.14 (6)
Mg	0.73 (2)	0.72 (3)	1.28 (4)	1.25 (3)	0.26 (2)	0.26 (2)	3.17 (9)	3.17 (11)
Mn	0.00	0.00	0.00	0.00	0.03 (1)	0.02 (2)	0.00	0.00
Σ	7.98	7.99	7.97	7.95	8.04	7.97	9.73	9.73
x_{Fe}	0.63	0.64	0.35	0.35	0.86	0.86	0.26	0.26

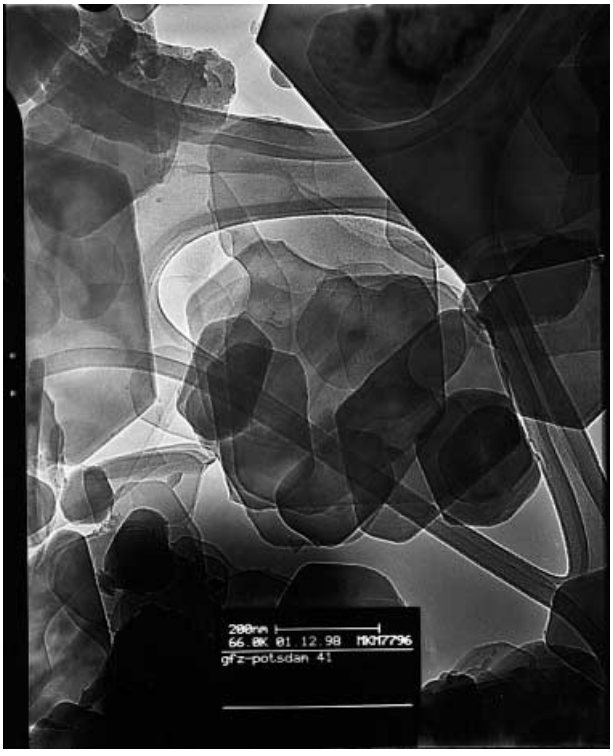

Fig. 2 TEM bright field image of run product 98-41 showing chlorite and chloritoid, both with hexagonal crystal shape

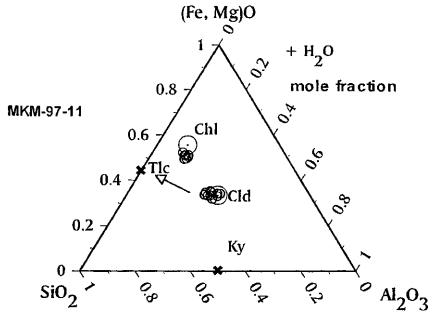

Fig. 3 Presentation of the compositions of the coexisting chlorite and chloritoid of run 97-11 (*small open circles*), together with ideal talc and kyanite composition indicating mixed chloritoid-talc analyses. Centres of *large open circles with dots* are ideal chloritoid and chlorite compositions

terials. The natural kyanite and talc samples are close to the end-member phases. The compositions and crystal chemistry of the chloritoids used in this study (except samples 97-17 and 98-23) are given in Koch-Müller et al. (2000). XRD revealed that chloritoid crystallises in the triclinic space group $C\bar{1}$, and that the Fe-Mg-chloritoid solid solution exhibits no excess volume. According to the Mössbauer spectra of the Fe-Mg chloritoids, the Fe^{3+} content is very low (1–4 wt% of the total Fe content) and can be neglected for the Mg-rich chloritoids used in the exchange runs. As discussed in Koch-Müller et al. (2000), the run products of some Mg-rich chloritoid contain staurolite, quartz and/or corundum as additional phases. The relatively coarse-grained quartz and corundum crystals could be removed from the starting material by hand under a stereomicroscope, but not the staurolite. Thus, some of the final mixture contains 1–2 mol% staurolite in addition to kyanite, chlorite, talc and chloritoid. The staurolite crystals did not react during the runs, and we assumed that its presence had no effect on reaction (1).

Only the most Mg-rich chlorites shown in Table 3 were used as starting material (97-1, 97-9, 99-2) for the exchange runs. These chlorites are close to the ideal formula $(Mg,Fe)_5Al[AlSi_3O_{10}/(OH)_8]$, representing clinochlore-chamosite solid solutions (Bailey 1988). Zane et al. (1998) present new classification diagrams for rock-forming chlorites based on an analytical study of more than 2,600 natural chlorites from amphibolite- and greenschist-facies rocks. According to their study the three main substitutions in chlorite are (1) the Tschermak substitution (e.g. $^{IV}Al^{VI}AlSi_{-1}Mg_{-1}$ in the MASH system), (2) the di-octahedral substitution Al_2Mg_{-3}, which produces vacancies in the sheets of octahedra (see also Foster 1962), and (3) the $FeMg_{-1}$ substitution. In the synthetic chlorites of this study, especially in the most Mg-rich chlorite used in the exchange runs, the extent of substitutions (1) and (2) is low and lies in the range observed for natural metapelitic chlorites (Zane et al. 1998; Table 3).

The structures of the chlorites were refined in the triclinic space group $C\bar{1}$ corresponding to the IIb-4 polytype (Bailey 1988). Starting values were the fractional atomic coordinates and the isotropic displacement parameters as determined by Phillips et al. (1980). The fractional site populations were constrained to the data obtained in the electron microprobe analyses under the following assumptions: random distribution of Si and Al over the two tetrahedral sites; ordering of Al at M4; random distribution of Fe, Mg and the remaining Al^{VI} over the M1-M3 sites (e.g. Joswig et al. 1980; Phillips et al. 1980). The number of profile parameters was 20–22, consisting of 14–16 background parameters, 4–6 parameters to define the variation of peak width with 2 Θ, and the peak shape. Texture effects due to the preferred orientation of the chlorite plates were corrected in the refinements, using the formalism of March (1932) and Dollase (1986). After convergence of the overall parameters (background, scale factor, lattice constants, profile parameters, and parameters to correct for preferred orientation), the atomic coordinates were refined – isotropic displacement parameters as well as the site-occupancy factors were constrained to the starting values. With increasing Fe content, the Si content of the chlorites decreases and olivine occurs as additional phase (98-14). In this case a quantitative phase analysis was performed with the structural input data, referring to the International Crystallographic Structural Database (ICSD). The refined lattice constants and molar volumes of some chlorites are given at the bottom of Table 3. The data indicate a linear relation between composition $x_{Fe} = Fe/(Fe+Mg)$ and molar volume of the chlorites:

Table 3 Electron microprobe analysis of the starting material kyanite, talc, synthetic chlorite (plus lattice parameter) and some chloritoid. The number of cations were calculated on the basis of 5, 11 and 14 oxygens (ky, tlc, chl) and 6 octahedral cations (cld) *Values in parentheses* 1 σ standard deviation

	Kyanite[a]	Talc[b]	97–1[c] Chl	97–9[c] Chl	98–10 Chl	99–1 Chl	98–14[d] Chl	98–37[e] Chl	97–17 Cld	98–23 Cld
SiO_2 (wt%)	37.03 (14)	62.09 (70)	30.77 (67)	26.20 (80)	30.02 (75)	31.22 (79)	24.82 (66)	22.79 (44)	25.77 (35)	25.84 (66)
Al_2O_3 (wt%)	63.11 (9)	0.22 (4)	17.97 (30)	17.55 (50)	17.82 (23)	19.87 (40)	20.57 (100)	20.02 (44)	41.97 (67)	40.44 (99)
FeO (wt%)	0.00	1.23 (10)[f]	0.00	4.51 (30)[f]	12.53 (38)[f]	12.61 (71)[f]	27.86 (40)[f]	37.10 (99)[f]	11.70 (25)	10.15 (43)
Fe_2O_3 [wt%]	0.17 (4)	–	–	–	–	–	–	–	0.27 (11)	0.44 (21)
MgO (wt%)	0.03 (1)	30.35 (57)	31.18 (55)	26.61 (34)	24.98 (83)	21.39 (65)	9.81 (20)	5.38 (14)	10.03 (30)	10.41 (35)
Σ	100.34	95.64	79.92	74.87	85.35	86.00	83.00	85.39	89.70	87.24
Si	1.00 (1)	3.99 (1)	3.08 (5)	2.89 (2)	3.02 (5)	3.10 (2)	2.89 (10)	2.66 (2)	2.08 (3)	2.15 (4)
$Al^{[4]}$	–	0.02 (1)	0.92 (3)	1.11 (2)	0.98 (2)	0.90 (4)	1.11 (7)	1.34 (2)	–	–
$Al^{[6]}$	2.00 (1)	–	1.20 (3)	1.17 (2)	1.13 (2)	1.43 (4)	1.63 (6)	1.41 (2)	3.99 (3)	3.97 (2)
Fe^{2+}	–	0.07 (1)	0.00	0.42 (3)	1.05 (3)	1.13 (4)	2.63 (3)	3.62 (5)	0.79 (2)	0.71 (1)
Fe^{3+}	0.00 (1)	–	–	–	–	–	–	–	0.01 (1)	0.03 (1)
Mg	0.00 (1)	2.91 (3)	4.70 (5)	4.38 (3)	3.74 (6)	3.17 (5)	1.65 (2)	0.94 (2)	1.21 (2)	1.29 (1)
Σ	2.99	6.99	9.86	9.97	9.93	9.73	9.82	9.97	8.08	8.15
x_{sud}	–	–	0.14	0.03	0.03	0.27	0.18	0.03	–	–
x_{Ts}	–	–	0.10	0.09	0.07	0.22	0.32	0.21	–	–
a_o (Å)	–	–	5.317 (1)	–	–	5.338 (1)	5.380 (1)	–	–	–
b_o (Å)	–	–	9.207 (2)	–	–	9.241 (2)	9.311 (2)	–	–	–
c_o (Å)	–	–	14.338 (3)	–	–	14.297 (3)	14.273 (3)	–	–	–
α (°)	–	–	90.22 (3)	–	–	90.19 (3)	90.13 (3)	–	–	–
β (°)	–	–	97.12 (3)	–	–	97.13 (3)	97.47 (3)	–	–	–
γ (°)	–	–	90.00 (3)	–	–	90.00 (3)	89.97 (3)	–	–	–
V_o (Å^3)	–	–	696.6 (3)	–	–	699.7 (3)	708.9 (3)	–	–	–

[a]Plus 0.03 wt% TiO_2, 0.03 wt% ZnO, 0.01 wt% MnO, and 0.03 wt% Cr_2O_3
[b]Plus 0.02 wt% TiO_2, 0.02 wt% ZnO, 0.03 wt% MnO, and 0.02 wt% Cr_2O_3
[c]Plus 4 wt% talc
[d]Plus 30–35 wt% olivine
[e]Starting material close to the real composition to avoid olivine growth
[f]Total iron as FeO

$V[Å^3] = 695.9 + 20.64 * x_{Fe}$

($r^2 = 0.98$). This is in excellent agreement with the relation given by McOnie et al. (1975) for monoclinic, synthetic Fe-Mg chlorites.

One Fe-rich chlorite (run no. 98-37, $x_{Fe} = 0.80$) was investigated by Mössbauer spectroscopy to check for the presence of Fe^{3+} in the synthetic chlorites. The Voigt-based analysis (Rancourt and Ping 1991) with two general quadrupole splitting distribution sites (Lorentzian FWHW = 0.29 mm s^{-1}) was applied to resolve the spectrum. Site 1, with an isomer shift (IS) of 1.12 ± 0.01 mm s^{-1} and a quadrupole splitting (QS) of 2.75 ± 0.01 mm s^{-1}, is assigned to Fe^{2+} in octahedral coordination (M1-M3 sites in chlorite). Site 2, with IS = 0.37 ± 0.03 mm s^{-1} and QS = 0.48 ± 0.06 mm s^{-1}, is assigned to Fe^{3+} in octahedral coordination (M4 site). The Voigt-based analysis of site 1 results in a Gaussian component σ_Δ of 0.17 mm s^{-1}. The relative amount of Fe^{3+} in the sample was about 3 ± 0.3% of Fe_{tot} – corresponding to 0.1 Fe^{3+} pfu. Thus, Fe^{3+} incorporation into the more magnesian chlorites of the exchange runs can be neglected.

Exchange runs

Table 4 shows the average mole fractions x_{Mg} and the observed range in x_{Mg} in chloritoid and chlorite after the runs. The changes of x_{Mg} in the run products is small but significant even for the very first analyses (97-11 and 97-13) where the number of useful analyses was low (9–12 per run product) due to strong phase overlap. The chemical compositions of the coexisting chlorite and chloritoid as well as of some talc minerals as determined by AEM are given in Tables 5 and 6.

The chlorites of the run products differ not only in the $FeMg_{-1}$ substitution from the starting material, but also in terms of the dioctahedral and Tschermak substitution. The extent of the dioctahedral substitution (x_{sud} = 6–Σoct. cations) in the chlorites varies in the range $x_{sud} = 0.20$–0.98, with an average value of 0.48 ± 0.22. The extent of the Tschermak substitution ($x_{Ts} = (Al^{VI} - 1)/2$) varies in the range $x_{Ts} = 0.16$–0.54, with an average value of 0.35 ± 0.14. The increase in the sudoite and Tschermak component in the product chlorites is significant but no dependence on P and/or T could be detected. For the thermodynamic estimates only run products with low x_{sud} and x_{Ts} were selected (97-13, 98-13).

As discussed above we were unable to determine the real composition of talc. The analyses of talc of run no. 98-42 are given in Table 6. In runs 97-13 and 98-41 similar compositions were observed. There is a strong positive correlation between the SiO_2 and MgO contents, a negative correlation between the SiO_2 and FeO (Al_2O_3), and the Si/Mg ratio is, in principle, too high for talc. The high Si content cannot be due to mixed analysis of talc with one or two of the other coexisting phases, since they are all poorer in silicon. Perhaps the analysis represents a mixture with quench SiO_2. The measured Al and Fe values could be caused by the surrounding Al- and Fe-bearing phases.

The AEM analyses performed on the product kyanite showed no increase of FeO during the runs. All kyanite crystals investigated contained less than 0.5 wt% FeO. Thus, in the thermodynamic analysis of the experiments we assumed that talc and kyanite did not change their compositions during the runs.

During the runs not only Fe and Mg exchange between chlorite and chloritoid but also a breakdown/growth of cld + tlc or chl + ky must have occurred. To estimate the direction and progress of reaction (1), we calculated the reaction coefficients for each run assuming that the bulk composition remains constant during the runs. Input data were the compositions of the coexisting products as determined by AEM (Table 4). In the calculations, the initial reaction coefficients 7 cld, 1 tlc, 2 chl and 5 ky were varied according to a simulated breakdown or growth of cld + tlc until the bulk composition of the specific exchange runs matches that of the starting material. An increase (decrease) of the reaction coefficients for cld and tlc with respect to the initial values indicates a breakdown (growth) of ky and chl, and vice versa for chl and ky. Zero or negative values for the reaction coefficients of cld plus tlc (chl plus ky) indicate that, with this bulk composition, the experiments would not be performed in the four-phase field but in the chl-ky field (cld + tlc field). The calculated reaction coefficients are given in Table 4. In all the runs the reaction coefficients deviate from the initial coefficients and yield positive coefficients for all four phases.

Except for a few cases, the existence of all four phases was proved by X-ray diffraction. However, in some runs the presence of talc could not be confirmed by X-ray diffraction since its amount was very low. In these cases its presence was proved and confirmed by optical examinations under a polarising microscope, and by electron microscopy and/or infrared spectroscopy. The IR spectra of chloritoid, chlorite and talc show intense, well-separated OH stretching bands at about 3,500, 3,580 and 3,680 cm^{-1} respectively. IR spectra of samples 98-25 and 98-42, which are both supposed to have a relatively low amount of talc, showed weak but significant bands at the characteristic wavenumber of 3,680 cm^{-1}.

In seven of eleven exchange runs the semiquantiative determination of the reaction direction indicates, for all three intensity ratios given above, the same directions and it was in agreement with the calculated reaction rate based on the bulk compositions (Table 4). In four runs, however, the results were not unequivocal. In the X-ray powder pattern of two runs (98-25 and 98-29), the intensity ratios $\frac{I^{cld}_{d(\bar{1}\bar{1}1)/(\bar{2}01)}}{I^{chl}_{d(002)}}$ and $\frac{I^{cld}_{d(\bar{1}\bar{1}1)/(\bar{2}01)}}{I^{chl}_{d(004)}}$ indicated growth of chloritoid plus talc whereas the intensity ratio $\frac{I^{cld}_{d(\bar{1}\bar{1}1)/(\bar{2}01)}}{I^{chl}_{d(201)}}$ indicates growth of chlorite plus kyanite. Growth of

Table 4 Results of the exchange runs (calculated reaction coefficients using the compositions of the products and assuming constant bulk compositions before and after the runs; the reaction coefficients were varied during the calculations according to a simulated breakdown or growth of cld + tlc until the bulk composition of the specific exchange runs matches that of the starting material). *Ns* Number of useful analyses

Run no.	Reactants		Products								
	x_{Mg}^{cld}	x_{Mg}^{chl}	x_{Mg}^{cld}	Range x_{Mg}^{cld}	x_{Mg}^{chl}	Range x_{Mg}^{cld}	K_D	Calculated reaction coefficients for cld + tlc = chl + ky[2]	Estimated reaction direction (X-ray)		
									$\frac{I_{d(\bar{1}\bar{1}1)/(\bar{2}01)}^{cld}}{I_{d(002)}^{chl}}$	$\frac{I_{d(\bar{1}\bar{1}1)/(\bar{2}01)}^{cld}}{I_{d(004)}^{chl}}$	$\frac{I_{d(\bar{1}\bar{1}1)/(\bar{2}01)}^{cld}}{I_{d(201)}^{chl}}$
								Initial (7, 1, 2, 5)	cld + tlc = chl + ky 3.2	2.7	2.9
97-11	0.65 (1)	1.00 (0)	0.71 (1)	0.70–0.71 Ns = 4	0.93 (2)	0.90–0.94 Ns = 5	5.29	cld + tlc < chl + ky (5.6, 0.8, 2.4, 6)		–	
97-13	0.65 (1)	0.90 (2)	0.72 (1)	0.70–0.72 Ns = 6	0.92 (1)	0.91–0.94 Ns = 6	4.87	cld + tlc≫chl + ky (11.2, 1.6, 0.8, 2)	cld + tlc > chl + ky –	3.3	3.3
98-12	0.61 (1)	0.78 (2)	0.57 (2)	0.53–0.62 Ns = 9	0.83 (2)	0.78–0.86 Ns = 9	3.65	cld + tlc≫chl + ky (8.4, 1.2, 1.6, 4)	cld + tlc≫chl + ky 6.9	13.4	3.9
98-13	0.49 (1)	0.78 (2)	0.54 (3)	0.52–0.61 Ns = 16	0.87 (1)	0.85–0.88 Ns = 9	5.65	cld + tlc≫chl + ky (11.9, 1.7, 0.6, 1.5)	Not unequivocal 3.9	5.8	0.7
98-25	0.64 (1)	0.90 (2)	0.59 (3)	0.56–0.64 Ns = 18	0.84 (1)	0.83–0.86 Ns = 7	3.65	cld + tlc < chl + ky (2.1, 0.3, 3.4, 8.5)	Not unequivocal 4.3	6.2	0.9
98-26	0.56 (2)	0.78 (2)	0.53 (3)	0.51–0.57 Ns = 18	0.76 (2)	0.73–0.80 Ns = 20	2.89	cld + tlc < chl + ky (4.2, 0.6, 2.8, 7)	cld + tlc < chl + ky 2.1	2.4	1.5
99-7	0.40 (2)	0.74 (2)	0.42 (2)	0.40–0.47 Ns = 16	0.75 (1)	0.74–0.78 Ns = 13	4.19	cld + tlc > chl + ky (8.4, 1.2, 1.6, 4)	cld + tlc≫chl + ky 8.2	16.7	5.9
98-41	0.64 (1)	0.78 (20	0.58 (4)	0.54–0.64 Ns = 28	0.78 (3)	0.74–0.85 Ns = 25	2.57	cld + tlc≪chl + ky (3.5, 0.5, 3, 7.5)	cld + tlc≪chl + ky 2.5	2.8	0.7
98-42	0.43 (1)	1.00 (0)	0.48 (2)	0.45–0.53 Ns = 11	0.83 (1)	0.81–0.84 Ns = 11	5.10	cld + tlc≪chl + ky (2.1, 0.3, 2.4, 8.5)	cld + tlc≪chl + ky 1.8	2.3	0.7
98-27	0.64 (1)	0.90 (2)	0.61 (2)	0.58–0.62 Ns = 10	0.86 (2)	0.85–0.86 Ns = 4	3.96	cld + tlc≪chl + ky (3.5, 0.5, 3, 7.5)	cld + tlc≪chl + ky 1.8	2.5	0.8
98-29	0.56 (2)	0.78 (2)	0.53 (2)	0.49–0.54 Ns = 32	0.78 (2)	0.75–0.82 Ns = 21	3.14	cld + tlc < chl + ky (5.6, 0.8, 2.6, 6)	Not unequivocal 3.4	6.25	1.2
99-5	0.40 (2)	0.74 (2)	0.45 (1)	0.42–0.46 Ns = 9	0.70 (2)	0.67–0.73 Ns = 11	2.92	cld + tlc > chl + ky (7.35, 1.05, 1.9, 4.75)	Not unequivocal 4.6	5.0	2.4

Table 5 AEM analyses of the products for runs 97-11, 97-13, 98-12, 98-13, 98-25, 98-26, and 99-07. The cations pfu were calculated on the basis of 14 oxygens (chl), 6 octahedral cations (cld)

Run no.	97-11		97-13		98-12		98-13		98-25		98-26		99-07	
	Chl	Cld	Chl	Cld	Chl	Cld	Chl	Cld	Chl	Cld	Chl	Cld	Chl	Cld
wt%														
SiO_2	39.2	29.10	38.1	28.9	45.1	29.4	37.1	30.6	37.2	28.8	37.2	29.4	44.8	28.5
Al_2O_3	22.9	47.6	27.7	50.1	26.0	46.8	22.8	45.1	28.3	43.5	28.3	47.5	28.7	45.6
FeO	4.6	10.1	4.3	8.7	7.3	13.7	8.6	14.7	8.7	20.9	8.7	12.9	9.8	18.4
MgO	33.2	13.3	29.9	12.4	21.5	10.0	31.5	9.6	25.8	8.8	25.8	10.4	16.7	7.5
Σ	100.0	100.0	100.0	100.0	100.0	99.9	100.0	100.0	100.0	99.9	100.0	99.9	100.0	100.0
apfu														
Si	3.19	2.07	3.08	2.05	3.62	2.16	3.08	2.30	3.06	2.15	3.23	2.15	3.62	2.13
$Al^{(4)}$	0.81	0.00	0.92	0.00	0.38	0.00	0.92	0.00	0.94	0.00	0.77	0.00	0.38	0.00
$Al^{(6)}$	1.38	3.99	1.72	4.18	2.08	4.05	1.31	3.99	1.81	4.09	1.54	4.06	2.35	4.02
Fe^{2+}	0.31	0.59	0.29	0.51	0.50	0.84	0.59	0.91	0.60	0.78	0.96	0.91	0.66	1.14
Mg	4.01	1.41	3.60	1.31	2.57	1.10	3.89	1.08	3.17	1.12	3.12	1.02	2.01	0.83
Σ	9.72	8.07	9.61	8.05	9.15	8.16	9.80	8.30	9.57	8.15	9.61	8.15	9.02	8.13
x_{sud}	0.28	–	0.40	–	0.85	–	0.20	–	0.43	–	0.39	–	0.98	–
x_{Ts}	0.19	–	0.36	–	0.54	–	0.16	–	0.41	–	0.27	–	0.68	–
x_{Fe}	0.07	0.29	0.07	0.28	0.16	0.43	0.13	0.46	0.16	0.41	0.24	0.47	0.25	0.58

chlorite and kyanite was in these cases also indicated by the calculations. Here, we believe more in the results of the $\frac{I^{cld}_{d(\bar{1}\bar{1}1)/(\bar{2}01)}}{I^{chl}_{d(201)}}$ ratio, since the intensity of the $d_{(201)}$ peak should be less orientation dependent than the intensities of the $d_{(002)}$ and $d_{(004)}$ peaks. Analyses of X-ray diffractograms of runs 98-13 and 99-5 yield contradictory results. Here, the calculations indicate growth of cld and tlc, as does the intensity ratios of $\frac{I^{cld}_{d(\bar{1}\bar{1}1)/(\bar{2}01)}}{I^{chl}_{d(002)}}\frac{I^{cld}_{d(\bar{1}\bar{1}1)/(\bar{2}01)}}{I^{chl}_{d(004)}}$. The intensity ratio of $\frac{I^{cld}_{d(\bar{1}\bar{1}1)/(\bar{2}01)}}{I^{chl}_{d(201)}}$ indicates growth of chlorite plus kyanite. Nevertheless, the X-ray analyses of all run products confirmed that the runs were performed in the four-phase field – although for some runs very close to the cld-tlc and chl-ky field boundaries.

As expected (e.g. Thompson 1976) and observed in nature (e.g. Vidal et al. 1999), chlorite solid solutions were always richer in magnesium than the coexisting chloritoid solid solutions. Incorporation of Fe into the chloritoid and chlorite phases extended the stability field of the assemblage chloritoid plus talc to lower pressures (Fig. 4a, b). The widths of the four-phase fields are defined by the compositions of chlorite and chloritoid which coexist together with kyanite and talc. Thus, the widths are controlled by the fractionation of iron and magnesium between chlorite and chloritoid according to reaction (EX).

The univariant Mg end-member reaction (1) has not been determined in this study. There are two thermodynamic data sets (Simon et al. 1997; Vidal et al. 1999) which both were extracted by Brian E. Patrick (see discussion in Vidal et al. 1999), using the experimental reversals of Chopin and Schreyer (1983), and Chopin (1985) in addition to other experimental data. The thermodynamic data for magnesiochloritoid from both data sets differ – mainly in the entropy values. Calculations using the program package Ge0-Calc (Brown et al. 1988), the thermodynamic data set of Berman (1988, updated), and the data set given in Simon et al. (1997) fit the experimental brackets and half-brackets for reaction (1) determined by Chopin (1985) better than that given in Vidal et al. (1999). $V_4 10^8 (K^{-2})$ given in Vidal et al. (1999) should read 0.001222; see also Goffé and Bousquet (1997). The entropy for chloritoid value given in Simon et al. (1997) is 131.9 J mol^{-1} K^{-1}, not 128.5 as reported in Vidal et al. (1999). In calculations using the data set given in Vidal et al. (1999), reaction (1) is shifted to higher pressures and has a flatter slope than shown in Fig. 1 (see below). Since the calculations based on the data of Simon et al. (1997) match the experimental data of Chopin (1985) best, we chose these calculated P-T coordinates as reference points in the MASH system in Fig. 4a and b. Nevertheless, the P–T coordinates calculated with Berman's data base and the data set of Vidal et al. (1999) are also in good agreement with our experiments. Calculations using the Holland and Powell (1998) data base yielded pressures which were much too high, at least compared with the experiments at 600 °C. The scatter in the data points of Fig. 4b indicates that the reaction is very sluggish at 540 °C, and equilibrium is difficult to reach. Therefore, the data obtained at 600 °C are of better quality.

Fe-Mg partitioning

The fractionation of Fe and Mg between chlorite and chloritoid as a function of pressure, temperature and composition is controversially discussed in the literature.

1. From an analysis of natural coexisting chloritoids and chlorites, Theye et al. (1992), and Azañón and Goffé (1997) suggested that the distribution coeffi-

Table 6 AEM analyses of the products for runs 98-41, 98-42, 98-27, 98-29 and 99-05. The cations pfu were calculated on the basis of 14 oxygens (chl), 6 octahedral cations (cld), and 11 oxygens (tlc)

Run no.	98–41		98–42						98–27		98–29		99–05	
	Chl	Cld	Tlc	Tlc	Tlc	Tlc	Chl	Cld	Chl	Cld	Chl	Cld	Chl	Cld
wt%														
SiO_2	38.3	29.4	71.5	71.0	70.2	61.3	40.4	29.4	38.4	29.8	37.8	29.5	39.3	29.0
Al_2O_3	23.7	46.4	0.9	1.8	1.8	7.3	24.4	45.4	27.2	47.0	24.5	46.3	22.0	44.6
FeO	12.7	13.7	2.7	2.1	2.2	9.6	9.6	16.8	8.1	12.5	12.7	14.8	16.6	18.5
MgO	25.3	10.4	24.9	25.0	25.8	21.7	25.6	8.4	26.3	10.7	25.0	9.4	22.1	10.0
Σ	100.0	100.0	100.0	100.0	100.0	100.0	100.0	100.0	100.0	100.0	100.0	100.0	100.0	100.0
apfu														
Si	3.22	2.15	4.28	4.24	4.20	3.83	3.32	2.20	3.14	2.18	3.17	2.19	3.35	2.17
$Al^{(4)}$	0.78	0.00	–	–	–	–	0.68	0.00	0.86	0.00	0.83	0.00	0.65	0.00
$Al^{(6)}$	1.56	4.00	0.06	0.13	0.13	0.54	1.69	4.00	1.77	4.06	1.59	4.04	1.55	3.95
Fe^{2+}	0.90	0.83	0.13	0.10	0.11	0.50	0.66	1.04	0.56	0.76	0.90	0.92	1.19	1.10
Mg	3.16	1.15	2.22	2.22	2.31	2.02	3.14	0.94	3.22	1.17	3.13	1.03	2.81	0.89
Σ	9.60	8.15	6.70	6.70	6.73	6.90	9.49	8.20	9.54	8.18	9.62	8.19	9.55	8.17
x_{sud}	0.40	–	–	–	–	–	0.51	–	0.46	–	0.38	–	0.45	–
x_{Ts}	0.28	–	–	–	–	–	0.34	–	0.39	–	0.29	–	0.28	–
x_{Fe}	0.22	0.42	–	–	–	–	0.17	0.53	0.15	0.39	0.22	0.47	0.30	0.55

cient $K_D^{cld/chl} = \frac{x_{Fe}^{cld} x_{Mg}^{chl}}{x_{Mg}^{cld} x_{Fe}^{chl}}$ increases slightly with pressure. Mazzoli and Peruzzo (1997) also observed that $K_D^{cld/chl}$ of natural cld-chl-bearing mineral assemblages is dependent on pressure, and proposed a potential geobarometer.

Factors which control the pressure dependence of the distribution coefficients are the magnitude of the volume of reaction ΔV_{EX}, the existence of an excess volume in one or both phases and/or changing mineral chemistry of one or both phases with pressure. As shown by Vidal et al. (1999), the volume of reaction ΔV_{EX} is very small (0.024 J bar^{-1}). In addition, cld and chl show no excess volume (McOnie et al. 1975; Chopin et al. 1992; Koch-Müller et al. 2000). Thus, the variation of $K_D^{cld/chl}$ with pressure observed by the authors mentioned above could reflect the dependence of $K_D^{cld/chl}$ on composition since, with increasing metamorphic grade (mainly pressure), both chlorite and chloritoid change their chemistry to more Mg-rich compositions (e.g. Chopin and Schreyer 1983; Chopin 1990; Spear 1995; Mazzoli and Peruzzo 1997; Simon et al. 1997).

2. Ghent et al. (1987) observed a decrease in $\ln K_D^{cld/chl}$ with increasing temperature. Since the variation is not very large, they proposed it as a relative temperature indicator and not as quantitative geothermometer. Vidal et al. (1999) analysed the pressure and temperature dependence of $K_D^{cld/chl}$, using 112 natural chloritoid-chlorite pairs from 28 different localities – mainly taken from dependence of $K_D^{cld/chl}$ on temperature. Their proposed empirical chloritoid-chlorite Fe-Mg exchange thermometer works for chlorite and chloritoid compositions which are not too close to the Fe- and Mg-end members ($0.2 < x_{Mg\text{-}cld} < 0.8$ at 700 °C, and $0.1 < x_{Mg\text{-}cld} < 0.9$ at 300 °C).
3. In most studies dealing with the Fe-Mg fractionation between cld and chl, ideal Fe-Mg mixing behaviour in both minerals has been assumed (e.g. Meyer 1983; Simon et al. 1997; Messiga et al. 1999). For clinochlore-chamosite solid solutions, ideal behaviour has been confirmed experimentally (Bryndzia and Scott 1987; Saccocia and Seyfried 1994), but not for chloritoids. On the contrary, spectroscopic studies on synthetic cld (Koch-Müller et al. 2000) indicated a nonideal mixing behaviour of cld.

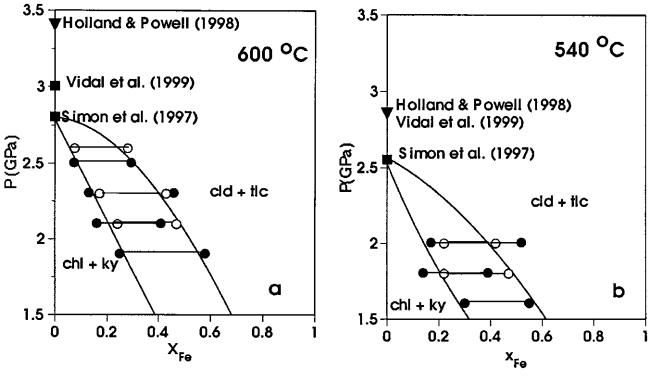

Fig. 4a–b Pressure-composition projections of the FMASH system showing the experimentally determined compositions of chlorite (*circles on the left*) and chloritoid (*circles on the right*) which coexist with kyanite and talc at **a** 600 and **b** 540 °C. *Open* (*closed*) *circles* Runs in which $K_D^{cld/chl} = \frac{x_{Fe}^{cld} x_{Mg}^{chl}}{x_{Mg}^{cld} x_{Fe}^{chl}}$ had increased (decreased) after the experiments. *Squares* and *triangles* Isothermal invariant points of the Mg end-member reaction (1) as calculated with thermodynamic data given by Simon et al. (1997), Vidal et al. (1999), and Holland and Powell (1998). *Solid lines* Fits through data points representing borders of the four-phase fields

Figure 5 shows the variation of $\ln K_D$ in selected exchange runs of this study (600 °C), together with data taken from literature as a function of temperature (Fig. 5a), pressure (Fig. 5b) and composition (Fig. 5c, d). The literature sources used are listed in Appendix 1. The selection is based on a critical evaluation of literature data by Vidal et al. (1999). The dependence

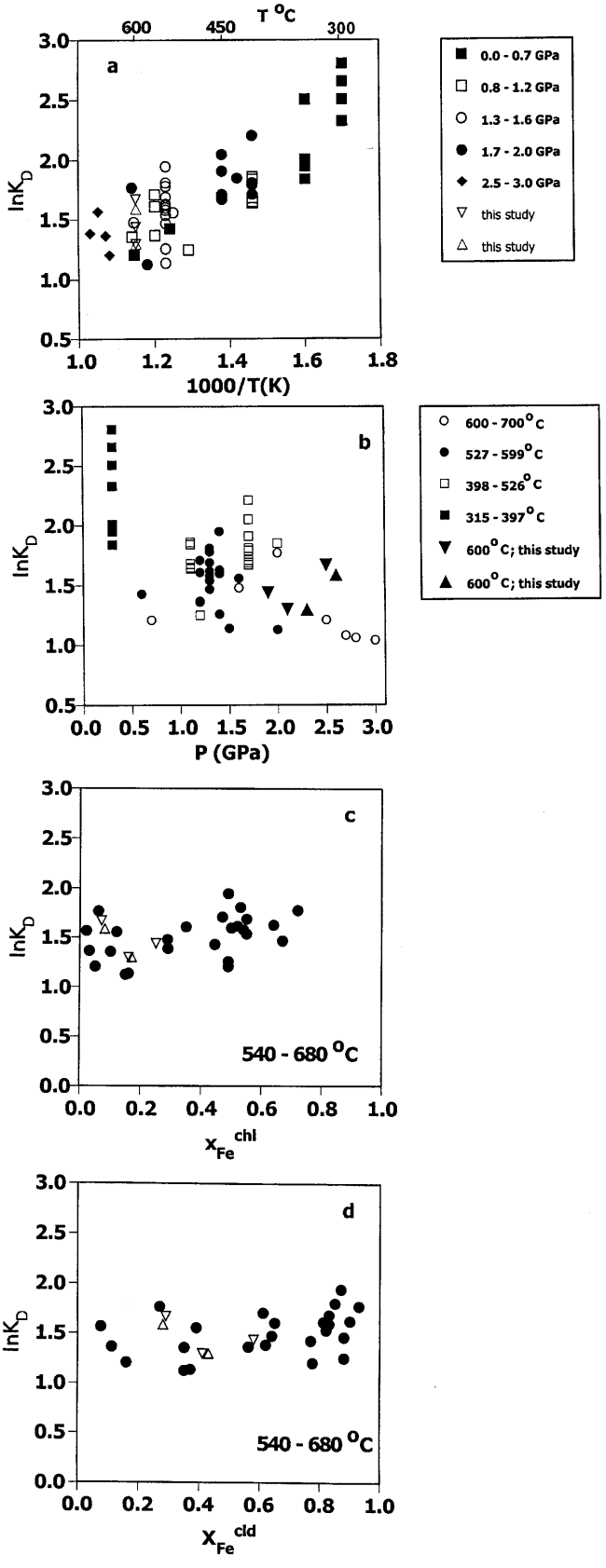

◀

Fig. 5a–d Variation of $lnK_D^{cld/chl}$ with **a** temperature, **b** pressure, and **c**, **d** composition. *Triangles* and *inverted triangles* Experimental results of this study using low-$K_D^{cld/chl}$ and high-$K_D^{cld/chl}$ starting compositions, respectively. *Remainder symbols* $lnK_D^{cld/chl}$-values of natural coexisting cld-chl pairs (data from Appendix 1)

of $lnK_D^{cld/chl}$ on temperature is obvious (Fig. 5a). $LnK_D^{cld/chl}$ decreases with increasing temperature. However, there is much scatter in the data points which cannot be related to the different equilibrium pressures for the assemblages (Fig. 5a). The effect of pressure on $lnK_D^{cld/chl}$ is shown in Fig. 5b. At low temperatures (< 530 °C) no effect of pressure $lnK_D^{cld/chl}$ can be observed. For the high temperature assemblages there could be a negative correlation of lnK_D with pressure. This is, however, not reflected by our experimental data points.

The large scatter in the $lnK_D^{cld/chl}$ versus 1/T diagram or the absence of a correlation with pressure could reflect an additional dependence of $lnK_D^{cld/chl}$ on composition. Figure 5c and d show plots of $lnK_D^{cld/chl}$ versus x_{Fe}^{chl} and x_{Fe}^{cld} respectively, for cld/chl pairs of a limited temperature range from 540 to 680 °C – but again no correlation can be observed. All of the experimental data points of this study lie in the Mg-rich part and show $lnK_D^{cld/chl}$ values comparable to those of the natural Mg-rich samples (Fig. 5c, d). The experimental brackets of this study indicate a slight decrease of lnK_D with increasing x_{Fe} in the Mg-rich part of the system. However, natural and experimental data points together scatter too much to permit a thermodynamic analysis. The scatter may be due to different extents in the Tschermak and/or dioctahedral substitutions in the natural chlorite samples.

The experimental data points at 600 °C of this study at least allow an estimate of the mixing behaviour in chloritoid. For these thermodynamic estimates, only run products with low x_{sud} and x_{Ts} were selected (97-13, 98-13). Figure 6 shows the position of the univariant reaction (1) in the MASH system, and the shift of the reaction lines with x_{Fe}^{cld} in the FMASH system. In Fig. 6a the Mg-end-member reaction (1) was calculated using the program package Ge0-Calc (Brown et al. 1988) and the thermodynamic data set of Berman (1988, updated), in addition to data for magnesiochloritoid given in Simon et al. (1997). Figure 6b shows the same reaction but calculated with data for magnesiochloritoid given in Vidal et al. (1999). The P-T coordinates of reaction (1) in the FMASH system have been calculated for both data sets with the experimentally determined compositions of runs 97-13 and 98-13, assuming ideal Fe-Mg mixing in choritoid and chlorite. For simplicity we supposed that, within the small P and T range shown in Fig. 6, the compositions of the coexisting chloritoid and chlorite do not change along the reaction lines as a function of P and T. In both calculations (Fig. 6a, b), the experimentally de-

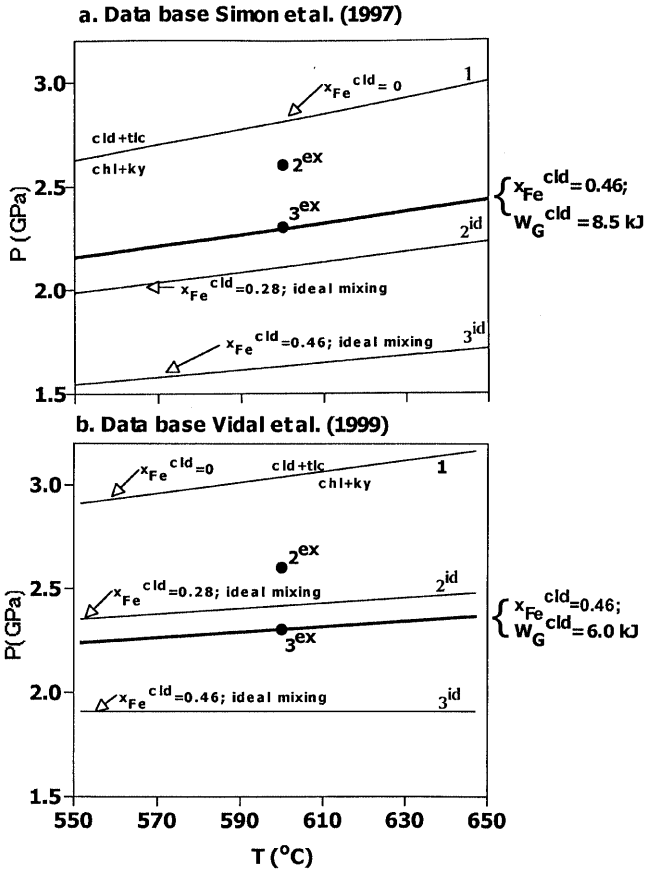

Fig. 6a–b Pressure-temperature diagrams showing the cld + tlc = chl + ky reaction as a function of x_{Fe}^{cld} calculated with the Ge0Calc software (Brown et al. 1988). Univariant *curves 1* Mg-end-member reaction (1) calculated using the thermodynamic data given by **a** Simon et al. (1997), and **b** Vidal et al. (1999). *Solid circles* 2^{ex} and 3^{ex} in both figures Experimentally determined pressures of runs 97-13 and 98-13 respectively, at 600 °C. *Isoplets* 2^{id} and 3^{id} Calculated using the experimentally determined compositions of cld and chl coexisting with talc and kyanite of runs 97-13 and 98-13 respectively, assuming ideal mixing behaviour in chloritoid and chlorite solid solutions. *Thick solid curves* Calculated isoplets using the results of run 98-13 under the assumption of symmetric mixing in chloritoid with an interaction parameter W_G of **a** 8.5 kJ, and **b** 6.0 kJ, and ideal Fe-Mg mixing in chlorite

termined P-T coordinates for the runs (2^{ex} and 3^{ex}, respectively) do not lie on the calculated isopleths, indicating a nonideal mixing behaviour of at least one phase, most probably chloritoid. The experimental data point 3^{ex} was used to estimate the direction and magnitude of the deviation from ideality for chloritoid solid solutions because the chlorite composition of this run was very close to the ideal clinochlore composition. The thick line in Fig. 6a shows the position of reaction (1) calculated under the assumption described above but assuming an interaction parameter $W_G = 8.5$ kJ for chloritoid solid solutions instead of ideal mixing behaviour. Figure 6b shows a similar calculation based on the thermodynamic data given in Vidal et al. (1999) and an interaction parameter of $W_G = 6.0$ kJ for chloritoid. In both cases, the experimentally determined P-T coordinates of run 98-13 lie exactly on the calculated curves. Thus, both calculations indicate a positive moderate deviation of Fe-Mg chloritoid from ideality – under the assumption of ideal Fe-Mg mixing in chlorite. The calculations were performed assuming $a_{Mg}^{tlc} = 1$, since we were unable to measure the real talc composition. If the activity of Mg in talc were less than one (e.g. $a_{Mg} = 0.96$ in Simon et al. 1997), the positive deviation from ideality for chloritoid solid solution would even increase.

Conclusions

1. The experiments show that incorporation of Fe into clinochlore and magnesiochloritoid coexisting with kyanite and talc (according to chl + ky = cld + tlc) extends the stability field of cld + tlc significantly towards lower pressures.
2. Analytical electron microscopy has successfully been applied to analyse the phase compositions in polyphase run products whose mineral compositions could otherwise only be determined by an indirect method.
3. Thermodynamic calculations based on data for magnesiochloritoid given by Simon et al. (1997), and those given in Vidal et al. (1999) in connection with Berman's data base are in good agreement with the experiments. Those given by Holland and Powell (1998) resulted in P coordinates for the Mg-end-member reaction which are much too high at 600 °C.
4. The experimental results suggest a positive, moderate deviation from ideality for chloritoid solid solutions.

Acknowledgements We thank H. Winkelmann for support in the high-pressure lab at the TU Berlin, and E. Schemmert, K. Paech, and I. Bauer for careful preparation of the samples for the different measurements. I. Abs-Wurmbach is thanked for providing access to the Mössbauer spectrometer. Helpful comments and advice were given by A. Feenstra and W. Heinrich on an early version of the manuscript. We thank the reviewers C. Chopin, T. Theye and O. Vidal, and the editor W. Schreyer for constructive and helpful suggestions.

Appendix

Sources of data used to calculate the $\ln K_D^{cld/chl}$ values of natural chl/cld pairs were the papers by Chinner and Dixon (1973), Miller (1977), Meyer (1983), Ashworth and Evirgen (1984), Chopin and Monié (1984), Ghent et al. (1987), Vuichard and Ballèvre (1988), El-Shazly and Liou (1991), Theye and Seidel (1991), Chopin et al. (1991), Theye et al. (1992), Okay and Kelley (1994), Faryad (1995), Engi et al. (1995), Azañón and Goffé (1997), Goffé and Bousquet (1997), Simon et al. (1997), and Vidal et al. (1999).

References

Ashworth JR, Evirgen MM (1984) Mineral chemistry of regional chloritoid assemblages in the chlorite zone, Lycian Nappes, south-west Turkey. Mineral Mag 347:159–165

Azañón JM, Goffé B (1997) Ferro- and magnesiocarpholite assemblages as record of high-P, low-T metamorphism in the central Alpujarrides, Betic Cordillera (SE Spain). Eur J Mineral 9:1035–1051

Bailey SW (1988) Chlorites: structures and crystal chemistry. In: Bayley SW (ed) Hydrous phyllosilicates. Rev Mineral 19:347–403

Bearth P (1963) Chloritoid und Paragonit aus der Ophiolit-Zone von Zermatt-Saas Fee. Schweiz Mineral Petrogr Mitt 43:269–286

Berman RG (1988) Internally-consistent thermodynamic data for minerals in the system Na_2O-K_2O-CaO-MgO-FeO-Fe_2O_3-Al_2O_3-SiO_2-TiO_2-H_2O-CO_2. J Petrol 29:445–522

Brown TH, Berman RG, Perkins EH (1988) GeO-Calc: software package for calculation and display of pressure-temperature-composition phase diagrams using an IBM or compatible personal computer. Comput Geosci 14:279–289

Bryndzia LT, Scott SD (1987) The composition of chlorite as a function of sulfur and oxygen fugacity: an experimental study. Am J Sci 287:50–76

Chinner GA, Dixon JE (1973) Some high-pressure parageneses of the Allalin gabbro, Valais, Switzerland. J Petrol 14:185–202

Chopin C (1983) Magnesiochloritoid, a key-mineral for the petrogenesis of high-grade pelitic blueschists. Bull Minéral 106:715–717

Chopin C (1985) Les relations de phases dans les metapelites de haute pression. PhD Thesis, Mém Sci Terre Université Curie, Paris, no 85–11

Chopin C (1990) Eclogite facies mineral parageneses. In: Carswell DA (ed) Eclogite facies rocks. Blackie, Glasgow, pp 35–42

Chopin C, Monié P (1984) A unique magnesiochlortoid-bearing, high-pressure assemblage from the Monte Rosa, Western Alps: petrologic and ^{40}Ar-^{39}Ar radiometric study. Contrib Mineral Petrol 87:388–398

Chopin C, Schreyer W (1983) Magnesiocarpholite and magnsiochloritoid: two index minerals of pelitic blueschists and their preliminary phase relations in the model system MgO-Al_2O_3-SiO_2-H_2O. Am J Sci 283(A):72–96

Chopin C, Henry C, Michard A (1991) Geology and petrology of the coesite-bearing terrain, Dora Maira massif, Western Alps. Eur J Mineral 3:263–291

Chopin C, Seidel E, Theye T, Ferraris G, Ivaldi G, Catti M (1992) Magnesiochloritoid, and the Fe-Mg series in the chloritoid group. Eur J Mineral 4:67–76

Cliff G, Lorimer GW (1975) The quantitative analysis of thin specimens. J Microsc 103:203–207

Dollase WA (1986) Correction of intensities for preferred orientations of the March model. J Appl Crystallogr 19:267–272

Dupas C, Doukhan N, Doukhan J-C, Green HW, Young TE (1994) Analytical electron microscopy study of a synthetic peridotite experimentally deformed in the β olivine stability field. J Geophys Res 99:15821–15832

Egerton RF (1996) Electron energy-loss spectroscopy in the electron microscope. Plenum Press, New York

El-Shazly AK, Liou JG (1991) Glaucophane chloritid-bearing assemblages from NE Oman: petrologic significance and a petrogenetic grid for high P metapelites. Contrib Mineral Petrol 107:180–201

Engi M, Todd CS, Schmatz DR (1995) Tertiary metamorphic conditions in the eastern Lepontine Alps. Schweiz Mineral Petrogr Mitt 75:347–369

Faryad SW (1995) Phase petrology and P-T conditions of mafic blueschists from the Meliata unit, West Carpathians, Slovakia. J Metamorph Geol 13:701–714

Foster MD (1962) Interpretation of the composition and a classification of the chlorites. US Geol Surv Prof Pap 414-A

Ghent ED, Stout MZ, Black PM, Brothers RN (1987) Chloritoid-bearing rocks associated with blueschists and eclogites, northern New Caledonia. J Metamorph Geol 5:239–254

Goffé B, Bousquet R (1997) Ferrocarpholite, chloritoid and lawsonite in metapelites of the Versoyen and Petit St Bernard units (Valais zone, Western Alps). Schweiz Mineral Petrogr Mitt 77:137–147

Holland TJB, Powell R (1998) An internally consistent thermodynamic data set for phases of petrological interest. J Metamorph Geol 16:309–343

Holland TJB, Baker J, Powell R (1998) Mixing properties and activity-composition and relationships of chlorites in the system MgO-FeO-Al_2O_3-SiO_2-H_2O. Eur J Mineral 10:395–406

Joswig W, Fuess H, Rothbauer R (1980) A neutron diffraction study of a one-layer triclinic chlorite (penninite). Am Mineral 65:349–352

Kiénast JM, Pognante U (1988) Chloritoid-bearing assemblages in eclogitized metagabbros from the Lanzo peridotite body (Western Italian Alps). Lithos 21:1–11

Koch-Müller M (1997) Experimentally determined Fe-Mg exchange between synthetic staurolite and garnet in the system MgO-FeO-Al_2O_3-SiO_2-H_2O. Lithos 41:185–212

Koch-Müller M, Abs-Wurmbach I, Langer K, Shaw C, Wirth R, Gottschalk M (2000) Synthetic and natural Fe-Mg-chloritoid: structural, spectroscopic and thermodynamic studies. Eur J Mineral 12:293–314

Kraus W, Nolze G (1999) PowderCell for Windows. Federal Institute for Materials Research and Testing, BAM, Berlin

Kretz R (1983) Symbols for rock-forming minerals. Am Mineral 68:277–279

Lagarec K, Rancourt DG (1998) Recoil. Mössbauer spectral analysis software for Windows. Department of Physics, University of Ottawa

Larson AC, van Dreele RB (1998) GSAS. General structure analysis system. Los Alamos National Laboratory, Los Alamos, NM 87545. Copyright The Regents of the University of California

Lorimer GW, Champness PE (1973) Combined electron microscopy and analysis of an orthopyroxene. Am Mineral 58:243–248

Malis T, Cheng SC, Egerton RF (1988) EELS log-ratio technique for specimens thickness measurements in the TEM. J Electron Microsc Tech 8:193–200

March A (1932) Mathematische Theorie der Regelung nach der Korngestalt bei affiner Deformation. Z Kristallogr 81:285–297

Martinez I, Wang Y, Guyot F, Liebermann RC, Doukhan JC (1997) Microstructures and iron partitioning in (Mg,Fe)SiO_3 perovskite–(Mg,Fe)O magnesiowüstite assemblages: an analytical transmission electron microscopy study. J Geophys Res 102(B3):5265–5280

Mazzoli C, Peruzzo L (1997) Fe-Mg distribution among the coexisting phases in chloritoid-bearing metapelites: a possible geobarometer. Terra Nova 9 Abstr Suppl 1:420

McOnie AW, Fawcett JJ, James RS (1975) The stability of intermediate chlorites of the clinochlore-daphnite series at 2 kbar P_{H2O}. Am Mineral 60:1047–1062

McPhail D, Berman RG, Greenwood HJ (1990) Experimental and theoretical constraints on aluminium substitutions in magnesian chlorite and a thermodynamic model for H_2O in magnesian cordierite. Can Mineral 28:859–874

Meissner E, Sharp TG, Chakraborty S (1998) Quantitative measurement of short compositional profiles using analytical transmission electron microscopy. Am Mineral 83:546–552

Messiga B, Scambelluri M, Piccardo GB (1995) Chloritoid-bearing assemblages in mafic systems and ecogite-facies hydration of alpine Mg-Al metagabbros (Erro-Tobbio Unit, Ligurian Western Alps). Eur J Mineral 7:1149–1167

Messiga B, Kienast JR, Rebay G, Riccardi P, Tribuzio R (1999) Cr-rich magnesiochloritoid eclogites from the Monviso ophiolites (Western Alps, Italy). J Metamorph Geol 17:287–299

Meyer J (1983) Mineralogie und Petrologie des Allalingabbros. PhD Thesis, University of Basel

Miller C (1977) Chemismus und phasenpetrologische Untersuchungen der Gesteine aus der Eklogitzone des Tauernfensters, Österreich. Tschermaks Mineral Petrogr Mitt 24:221–277

Okay AI, Kelley SP (1994) Tectonic setting, petrology and geochronology of jadeite + glaucophane and chloritoid + glaucophane schists from north-west Turkey. J Metamorphic Geol 12:455–466

Peacor DR (1993) Analytical electron microscopy: X-ray analysis. In: Buseck PR (ed) Minerals and reactions at the atomic scale: Transmission electron microscopy. Rev Mineral 27:113–140

Phillips TL, Loveless JK, Bailey SW (1980) Cr^{3+} coordination in chlorites: a structural study of ten chromian chlorites. Am Mineral 65:112–122

Platonov AN, Tarashchan AN, Langer K, Andrut M, Partzsch G, Matsyuk S (1998) Electronic absorption and luminescence spectroscopic studies of kyanite single crystals: differentiation between excitation of TiFe charge transfer and Cr3 + dd transitions. Phys Chem Minerals 25:203–221

Pouchou JL, Pichoir F (1985) ''PAP'' F (ρZ) procedure for improved quantitative microanalysis. Microbeam Anal 1985:104–106

Rancourt DG, Ping JY (1991) Voigt-based methods for arbitrary shape static hyperfine parameter distributions in Mössbauer spectroscopy. Nuclear Instr Methods Phys Res B58:85–97

Saccocia PJ, Seyfried W (1994) The solubility of chlorite solid solutions in 3.2 wt% NaCl fluids from 300 to 400 °C, 500 bars. Geochim Cosmochim Acta 58:567–585

Schreyer W (1988) Experimental studies on metamorphism of crustal rocks under mantle pressures. Mineral Mag 52:1–26

Simon G, Chopin C, Schenk V (1995) Granulite-facies overprint in ultrahigh-pressure rocks, Dora Maira Massif, Western Alps? Bochumer Geol Geotech Arb 44:224–227

Simon G, Chopin C, Schenk V (1997) Near-end-member magnesiochloritoid in prograde-zoned pyrope, Dora-Maira massif, western Alps. Lithos 41:37–57

Spear FS (1995) Metamorphic phase equilibria and pressure-temperature-time paths. Mineral Soc Am Monogr Ser

Theye T, Seidel E (1991) Petrology of low-grade high-pressure metapelites from the external Hellenides (Crete, Peloponnes). A case study with attention to sodic minerals. Eur J Mineral 3:343–366

Theye T, Seidel E, Vidal O (1992) Carpholite, sudoite, and chloritoid in low grade high-pressure metapelites from Crete and the Peloponnes, Greece. Eur J Mineral 4:487–507

Thompson A (1976) Mineral reactions in pelitic rocks. I. Prediction of P-T-X (Fe-Mg) phase relations. Am J Sci 276: 401–424

Vidal O, Goffé B, Bousquet R, Parra T (1999) Calibration and testing of an empirical chloritoid-chlorite Mg-Fe exchange thermometer and thermodynamic data for daphnite. J Metamorph Geol 17:25–39

Vuichard JP, Ballèvre M (1988) Garnet-chloritoid equilibria in eclogitic pelitic rocks from the Sesia zone (Western Alps): their bearing on phase relations in high pressure metapelites. J Metamorph Geol 6:135–157

Zane A, Sassi R, Guidotti C (1998) New data on metamorphic chlorite as a petrogenetic indicator mineral, with special regard to greenschist-facies rocks. Can Mineral 36: 713–726